ACS APPLIED MATERIALS & INTERFACES

Research Article

www.acsami.org

Carbon Nanotube Buckypaper Reinforced Acrylonitrile–Butadiene–Styrene Composites for Electronic Applications

Ana M. Díez-Pascual*,† and David Gascón‡

†Institute of Polymer Science and Technology (ICTP-CSIC), Juan de la Cierva 3, 28006 Madrid, Spain

‡Libelium, María de Luna 11 (Installations CEEI), 50018, Zaragoza, Spain

ABSTRACT: Novel acrylonitrile–butadiene–styrene (ABS) nanocomposites reinforced with pristine or functionalized single- or multiwalled carbon nanotube buckypaper (BP) sheets were manufactured via hot-compression and vacuum infiltration. Their morphology, thermal, mechanical, and electrical properties were comparatively investigated. Scanning electron microscopy and thermogravimetric analysis showed that the infiltration process leads to better BP impregnation than the hot-press technique. BPs made from functionalized or short nanotubes form compact networks that hamper the penetration of the matrix chains, whereas those composed of pristine tubes possess large pores that facilitate the polymer flow, resulting in composites with low degree of porosity and improved mechanical performance. Enhanced thermal and electrical properties are found for samples incorporating functionalized BPs since dense networks lead to more conductive pathways, and a stronger barrier effect to the diffusion of degradation products, thus better thermal stability. According to dynamic mechanical analysis these composites exhibit the highest glass transition temperatures, suggesting enhanced filler–matrix interactions as corroborated by the Raman spectra. The results presented herein demonstrate that the composite performance can be tailored by controlling the BP architecture and offer useful insights into the structure–property relationships of these materials to be used in electronic applications, particularly for EMI shielding and packaging of integrated circuits.

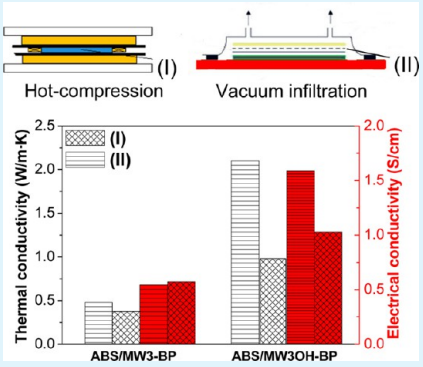

KEYWORDS: *buckypaper, ABS composites, impregnation, thermoelectrical properties, electronics*

1. INTRODUCTION

Composite materials have been traditionally developed for structural uses. However, with the rapid growth of the electronics industry, they are currently employed in a wide number of electronic applications. While structural composites require high stiffness and strength, electronic composites demand high thermal conductivity, low dielectric constant, high/low electrical conductivity, or electromagnetic interference (EMI) shielding effectiveness, depending on the particular appliance. High dimensional stability is another important aspect of electronic assemblies, which are frequently required to withstand high temperatures and moisture absorption while exhibiting little creep, warp or flex. Their processability into small parts and machineability are highly desirable while the product cost is not a limiting factor, thus it is feasible to incorporate expensive fillers. The applications of polymer based composites in this field include interconnections, printable circuit boards, substrates, encapsulations, interlayer dielectrics, die attach, electrical contacts, thermal interface materials, heat sinks, connectors, lids and housings, among others.[1]

Acrylonitrile–butadiene–styrene (ABS) is a widely used engineering thermoplastic positioned between commodity polymers and high performance plastics such as nylons. It possesses superior chemical properties, excellent toughness, high dimensional stability, and can be easily machined into products with excellent surface appearance at relatively low cost.[2] The structure of ABS is a matrix of styrene acrylonitrile copolymer (SAN) with a dispersion of rubbery polybutadiene (PB). Due to its flexibility of composition, this terpolymer exhibits a wide range of applications in electronic, automotive and domestic appliances. In particular, it is employed in automotive interior components including panels, consoles, radiator grills, headlight housings, and inner trim parts. ABS has been used as an additive to improve the toughness of engineering plastics, such as nylon-6 (PA-6),[3] poly(butylene terephthalate) (PBT),[4] and polycarbonate (PC).[5] ABS/PC blends exhibit an optimum balance of toughness, thermal stability, easy processability, and low cost, hence are the dominant polymeric material used in the electronics industry. ABS composites incorporating electrically conductive nanoscale fillers are interesting for developing EMI shielding materials and plastic sheets useful for packaging of integrated circuit devices. The primary mechanism of EMI shielding is reflection. Thus, the shield material should have mobile charge carriers (electrons or holes) that reflect the electromagnetic radiation, hence it needs to be electrically conductive, although a conductivity of 1 S/cm is normally sufficient.[1] For the packaging of electronic components, antistatic characteristics

Received: September 13, 2013
Accepted: October 30, 2013
Published: October 30, 2013

Table 1. Characteristics and Codes of the CNTs and the Corresponding Buckypapers[a]

CNT type	L (μm)	D (nm)	density (g/cm^3)	porosity[b] (%)	pore size[c] (nm)
MWCNT	10−30	10−30	0.34 ± 0.02	82 ± 4	180 ± 22
MWCNT	0.5−2.0	10−20	0.44 ± 0.04	76 ± 3	120 ± 15
SWCNT	5−30	1−2	0.17 ± 0.01	87 ± 5	250 ± 31
MWCNT-COOH	<10	10−30	0.65 ± 0.04	65 ± 3	40 ± 8
MWCNT-$CONH_2$	<10	10−30	0.50 ± 0.03	73 ± 4	60 ± 11
CNT type	FD[d] (%)	CR_{800}[e] (wt %)	T_i[d] (°C)	G/D ratio[f]	sample code
MWCNT		0.5 ± 0.03	>800	1.6 ± 0.2	MW3-BP
MWCNT		2.6 ± 0.06	682 ± 1	1.1 ± 0.1	MW7-BP
SWCNT		3.7 ± 0.09	635 ± 2	17.2 ± 0.9	SW1-BP
MWCNT-COOH	7.9 ± 0.5	0.1 ± 0.01	188 ± 1	0.53 ± 0.08	MW3OH-BP
MWCNT-$CONH_2$	3.2 ± 0.3	0.1 ± 0.02	252 ± 1	0.67 ± 0.09	MW3NH-BP

[a] L = nanotube length; D = nanotube diameter; FD = nanotube functionalization degree; CR = char residue at 800 °C; T_i = initial degradation temperature at 2% weight loss. [b] From density measurements. [c] Apparent average value from SEM. [d] From TGA measurements under inert atmosphere. [e] From TGA under air environment. [f] From Raman spectra.

are required since the circuits can be damaged by static electrical charges. Conductivities higher than 10^{-4} S/cm are suitable for electrostatic charge dissipation.[6] For this purpose, carbon black (CB)[7] and carbon nanotubes (CNTs)[8−10] have been incorporated into ABS, and the resulting composites showed electrical conductivities in the range of 10^{-3}−10^{-2} S/cm at filler loadings of 20 vol% and 1.3 wt %, respectively.

It is known that one of the major drawbacks in the development of polymer/CNT nanocomposites is the strong tendency of these nanofillers to form agglomerates, which hinders their homogeneous dispersion. Recently, CNT sheets also known as "buckypapers" (BPs) have been used as fillers for the preparation of composites to improve connectivity and prevent the appearance of regions without tubes.[11,12] BPs are free-standing thin porous networks of randomly entangled CNTs cohesively bound by van der Waals interactions. They are commonly prepared by dispersion of pristine or chemically modified nanotubes in a solvent medium and subsequent vacuum filtration through a microporous membrane.[13] It has been demonstrated that buckypaper film properties are affected by a wide number of parameters such as the CNT length, purity, diameter and number of walls, the chemical modification of the tubes, and their degree of alignment.[14,15] In addition, the solvent medium used for the CNT dispersion as well as the synthesis conditions (sonication time, final dispersion volume, type of membrane filter, etc) and post-treatments have a significant effect on the pore size distribution and nanotube packing density, hence on the final properties of the material.[16] A careful control of the aforementioned parameters influencing the BP structure is highly desirable for targeted applications.

BP composites can be fabricated by techniques such as hot-compression,[11] through-thickness infiltration,[12] electro-spinning,[17] and intercalation.[18,19] They typically have a carbon nanotube content higher than 30 wt %, resulting in a network which acts as an skeleton. In these composites, terms such as porosity, impregnation degree and quality of the BP-matrix interface are extremely important. To date, most of the studies focused on epoxy/BP composites,[20] albeit a few studies dealing with thermoplastic matrices like PC,[12] polyvinyl alcohol (PVA), polystyrene (PS), polyvinyl pyrrolidone (PVP),[18,19] poly(ether ether ketone) (PEEK), or polyphenylene sulphide (PPS)[11,21] have been reported.

The main objective of this work is to investigate the thermal and electrical properties of ABS/BP nanocomposites with a view to use them in the electronics industry, particularly for EMI shielding and packaging of integrated circuits. Since these applications have certain structural requirements, their mechanical performance has also been analyzed. For that purpose, different types of buckypapers were synthesized from CNTs with varying length (long or short), number of walls (single or multiwalled, SWCNTs or MWCNTs) and functionalization (pristine, amide or acid-functionalized). To the best of our knowledge, no previous systematic study on the effect of such parameters on the composite performance has been reported to date. Two different techniques, hot-press processing and another one based on vacuum infiltration were used to impregnate the BP sheets with the ABS matrix. The ultimate aim is to attain an in-depth understanding of the structure−property relationships to tailor the composite properties for the above-mentioned applications.

2. EXPERIMENTAL SECTION

Materials. ABS, a terpolymer of acrylonitrile (24%), butadiene (6%), and styrene (70%) was obtained from LG Chem Ltd. ($d_{25°C}$ = 1.05 g/cm^3, $T_g \approx 113$ °C, $\eta_{310°C} \approx 13\,200$ Pa·s). Catalytic chemical vapor deposition (CVD) pristine SWCNTs (SW1), long MWCNTs (MW3) and short MWCNTs (MW7) were supplied by Cheap Tubes Inc. (VT, USA). The characteristics of each type of nanotube are listed in Table 1. Tetrahydrofuran (THF, 99.9%), aqueous ammonia (NH_3, 1 M), nitric acid (HNO_3, 65%), dichloromethane (DCM, 99.8%), and thionyl chloride ($SOCl_2$, 99%) were purchased from Aldrich and used without further purification. *N,N*-dimethylformamide (DMF, 99%) obtained from Fluka, was distilled under vacuum and then dried for a few days with a Merck 4 Å molecular sieve.

Synthesis of Acid and Amide-Functionalized MWCNTs. Acid-functionalized MWCNTs were prepared by refluxing a small amount of nanotubes in HNO_3 1.5 M at 120 °C for 4 h under constant stirring, followed by sonication for 30 min and centrifugation at 5500 rpm for 15 min. This procedure under mild acid conditions was adopted to minimize damage of nanotube sidewall. Then, the supernatant was removed, and the solid was redispersed in H_2O/HCl at pH ∼2. After several sonication and centrifugation cycles, the resulting suspension was filtered through a PC membrane (1.2 μm pore size), rinsed with water until neutral and vacuum-dried in an oven at 60 °C for 24 h.

Concerning the amidation protocol, the acid-functionalized MWCNTs were submerged in anhydrous DMF and sonicated in an ultrasound bath for 15 min. Subsequently, an excess of $SOCl_2$ was added at 120 °C and the reaction was allowed to proceed for 18 h under reflux and constant stirring. The residual $SOCl_2$ was removed by reduced pressure distillation to yield acyl-chloride-functionalized MWCNTs. These were then reacted with aqueous ammonia 1 M at 80 °C for 24 h and dried under vacuum at 80 °C for 6 h.

The functionalization degree (FD) of the MWCNTs was calculated from thermogravimetric analysis (TGA) curves under nitrogen atmosphere according to the equation:[22] FD = [100 × L (%) × 12 g/mol]/[R (%) × M_w (g/mol)], where L (%) is the weight loss between 150 and 600 °C, R (%) is the residual mass at 600 °C, and M_w is the molecular weight of the desorbed moieties. The values obtained for acid and amide-functionalized MWCNTs are collected in Table 1.

Synthesis of Buckypapers. SWCNTs or MWCNTs (either pristine or functionalized) were ground in a small amount of THF with a mortar. Subsequently, the mixture was transferred to a beaker with ethanol and treated with an ultrasonic tip for about 1 h until a well dispersed suspension was attained, which was then filtered under vacuum through a PC membrane with a pore size of 0.45 μm. The wet BP was hot-pressed overnight between two metal plates and subsequently dried in an oven at 85 °C. The thickness of all BPs was in the range of 70−90 μm. Table 1 summarizes the characteristics and codes of the BPs synthesized in this work.

Manufacturing of Buckypaper-Reinforced ABS Composites. Prior to manufacturing, ABS and the BPs were placed in an oven at 100 °C for 24 h to remove solvents and absorbed moisture. Two different techniques were used for BP impregnation: hot-compression and vacuum infiltration. In the first procedure, ABS was extruded in a Haake Rheocord 90 system at 220 °C and a rotor speed of 150 rpm for 20 min. Afterward, steel shims were used to fabricate thin films (~0.15 mm) of the extruded material in a hot-press at 220 °C under high pressure. Subsequently, the nanocomposites were prepared by placing a BP sheet between two ABS films. Consolidation of the material was carried out at the same temperature in a hot-press under successive pressures of 10, 30, and 100 bar for periods of 5 min at each step. The consolidation cycle was optimized to minimize the internal porosity and to improve the impregnation of the BPs with the polymer resin. The composites prepared by this approach (hereafter designated as class I) were cut into small specimens for characterization; a few small pores (~0.5 mm diameter) were detected on their surface (Figure 1a).

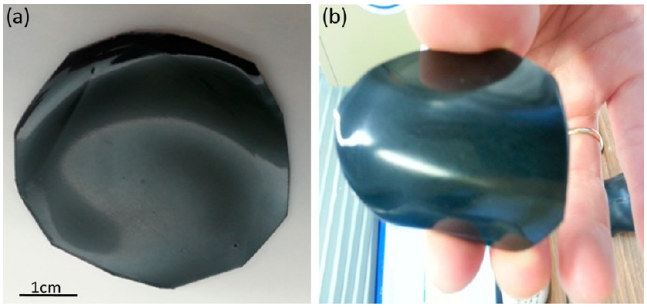

Figure 1. Photographs of ABS/MW3-BP nanocomposites prepared by hot-compression (a) and vacuum infiltration (b) processes.

In the second method, ABS was dissolved in DCM under vigorous mixing. The BPs were cut into rectangles and manually impregnated by pouring the resin solution on their top. A breather was employed to remove the solvent and the air from the BP, and a porous release film was located between the breather and the BP to separate the composite from the breather after impregnation. The whole system was then covered by a vacuum bag. Subsequently, reduced pressure of ~0.8 bar was applied to the system placed in a vacuum oven, and to ensure sufficient time for infiltration and remove the solvent, vacuum was maintained for 3 h at 100 °C. The resulting nanocomposites (hereafter named class II) showed a high degree of impregnation, with a uniform and smooth surface (Figure 1b).

Materials Characterization. The surface morphology of the synthesized BPs and the composites was analyzed with a Philips XL30 scanning electron microscope (SEM) equipped with an energy dispersive X-ray detector (EDAX), applying an acceleration voltage of 25 kV and an intensity of 9 × 10^{-9} A. To prevent charging during electron irradiation, samples were coated with a thin Au/Pd overlayer.

Raman spectra were acquired with an InVia Raman microscope (Renishaw), using a 785 nm (1.58 eV) laser excitation source and 50× magnification objective lens. Spectra were recorded by scanning the 100−3000 cm^{-1} region, with a typical incident laser power of 0.5 mW, resolution of 4 cm^{-1} and total acquisition time of 3 min.

The thermal stability of the samples and their residual weight were evaluated by TGA using a Mettler TA-4000/TG-50 thermobalance coupled to a mass spectrometer. The temperature was scanned from 25 to 800 °C at a heating rate of 10 °C/min under dry air and nitrogen atmospheres. Experiments were carried out on samples with an average mass of 20 mg, and the purge air or nitrogen flow rate was 50 mL/min. Three tests were performed on each sample to obtain an average weight measurement of the residues.

Dynamic mechanical tests were performed on a Mettler DMA 861 dynamic mechanical analyzer. Measurements were carried out in the tensile mode at frequencies of 0.1, 1, and 10 Hz, in the temperature range between −100 to 200 °C, at a heating rate of 2 °C/min. A dynamic force of 6 N was applied oscillating at fixed frequency and amplitude of 30 μm.

Quasi-static mechanical tests were carried out on a servo-hydraulic testing machine (type MTS 858) equipped with a temperature control system, using a crosshead speed of 1 mm/min and a load cell of 100 kN at 23 ± 2 °C and 50 ± 5% relative humidity. Tensile tests were performed according to ASTM D638 standard. All the samples were conditioned for 24 h before the measurements. Five coupons were tested for each sample, and the data reported correspond to the average value.

The room temperature electrical conductivity of the samples was measured by the four-point probe method using a Scientific Equipment device with a spacing probe S = 0.2 cm equipped with a DC precision power source (Model LCS-02) and a digital micro-voltmeter (Model DMV-001). The values reported correspond to the average of 6 measurements.

The thermal diffusivity (α) was measured by laser flash radiometry technique. A pulsed Nd:YAG laser with wavelength of 1.06 μm was used to heat the front surface of the sample. The thermal radiation from the rear surface was focused by germanium lens onto a liquid nitrogen cooled MCT (Mercury, Cadmium, Tellurium) infrared detector with response time of 40 ns and cutoff wavelength of 12.5 μm. The signals received by the detector were amplified and collected with a 500 M bandwidth TDS3052B oscillograph. Measurements were carried out by averaging over 20−100 laser shots. The averaged signals were recorded as a function of time and adjusted to fit the Clark-Taylor model.[23] The thermal conductivity (λ) at 25 °C was calculated according to the equation: $\lambda = \rho \times C_p \times \alpha$, where ρ and C_p are the density and specific heat capacity of the samples, respectively. At least 3 readings for each material were taken to ensure repeatability.

3. RESULTS AND DISCUSSION

Characterization of the Synthesized Buckypapers. TGA tests under oxidative environment were performed to determine the purity of BPs. A metallic residue lower than 5% was measured for all the samples (Table 1), arising from the metal catalyst particles (Ni, Co, Fe) used for the CNT synthesis. BPs incorporating functionalized MWCNTs hardly showed metallic impurities, since these were successfully removed during the treatment in nitric acid. Under inert environment, pristine MW3-BP starts to decompose (T_i) at temperatures higher than 800 °C, while MW7-BP and SW1-BP initiate the degradation at around 682 and 635 °C, respectively. Significantly lower thermal stability was found for MW3NH-BP and MW3OH-BP, because of the pyrolysis of the functional groups attached onto the nanotube sidewalls.

The average density of the buckypapers was calculated from measurements of their weight, thickness and surface area. Assuming a density of 1.3 g/cm^3 for SWCNT ropes[11] and 1.9 g/cm^3 for MWCNTs (calculated as the density of graphite

corrected by the ratio of the volume of the inner tube to that of the outer one),[24] the degree of porosity of these carbon nanomaterials was estimated as difference between the experimental and the theoretical density (Table 1). Interestingly, SW1-BP shows the highest void content, which might be related to the higher tendency of this type of nanotubes to form agglomerates due to strong van der Waals forces between individual tubes, hence the CNTs would be poorly exfoliated during the dispersion step prior to the vacuum filtration, and the resulting buckypaper develops large pores. Regarding the influence of the nanotube length, it is found that shorter MWCNTs lead to lower degree of porosity, since they can easily rearrange and form a densely packed network, in agreement with the results reported previously.[25] BPs containing functionalized MWCNTs display the lowest degree of porosity, since the oxidation treatment in acid medium is known to induce a shortening of the nanotubes.[26] Further, the hydrogen bonding forces between acid and amide groups located on the surface of adjacent tubes result in a more compact and structurally integrated buckypaper. Another crucial parameter that affects the BP packing density is the chemical affinity between the nanofillers and the solvent used for their exfoliation in solution. The polar groups of the functionalized MWCNTs should have stronger interactions with the ethanol used as dispersion medium than the hydrophobic pristine nanotubes, hence would be individually dispersed in solution, creating a very compact architecture after the filtration of the CNT suspension.

Analogous conclusions were drawn from SEM images (Figure 2). In all cases, a uniform morphology of the CNT network was observed, with randomly orientated tubes and a broad distribution of pore sizes. SEM images are useful for determining the BP pore diameter; however, the measured data should be regarded only as a rough estimation (apparent average values). Functionalized BPs present the smallest pores (Table 1), showing average apparent sizes of 40 and 60 nm for MW3OH-BP and MW3NH-BP, respectively. As can be observed in the image of MW3NH-BP (Figure 2a), the nanotubes are entangled and tightly arranged leaving only small free spaces among them, with a large number of interconnections between neighbor tubes. A completely different morphology is found for SW1-BP (Figure 2b), where the nanotubes seem more disentangled and appear to be in a foamy state, resulting in a loose network with fewer connections, hence lower mechanical integrity, and an average pore size of ~250 nm. An intermediate structure is observed for MW3-BP (Figure 2c), with a mean pore diameter of 180 nm. The BP packing density and pore size would greatly influence its permeability, hence the impregnation quality of the corresponding composites, as will be discussed in a following section. Small pore sizes are not appropriate for infusion of macromolecular chains within the network. The film must have large pores to allow complete matrix impregnation.

Figure 3 compares the Raman spectra for pristine and functionalized BPs. The spectrum of SW1-BP displays three characteristic peaks: a weak D band centered at ~1300 cm^{-1}, attributed to defects in the nanotube lattice including sp^3 hybridized carbon, an intense G band at ~1590 cm^{-1}, associated with tangential C−C bond stretching motions[27] and the G′ band (D overtone) at ~2590 cm^{-1}. The profile of the G band is characteristic of semiconducting SWCNTs.[26] The same bands were detected for BPs composed of MWCNTs, albeit slightly shifted to higher wavenumber and showing

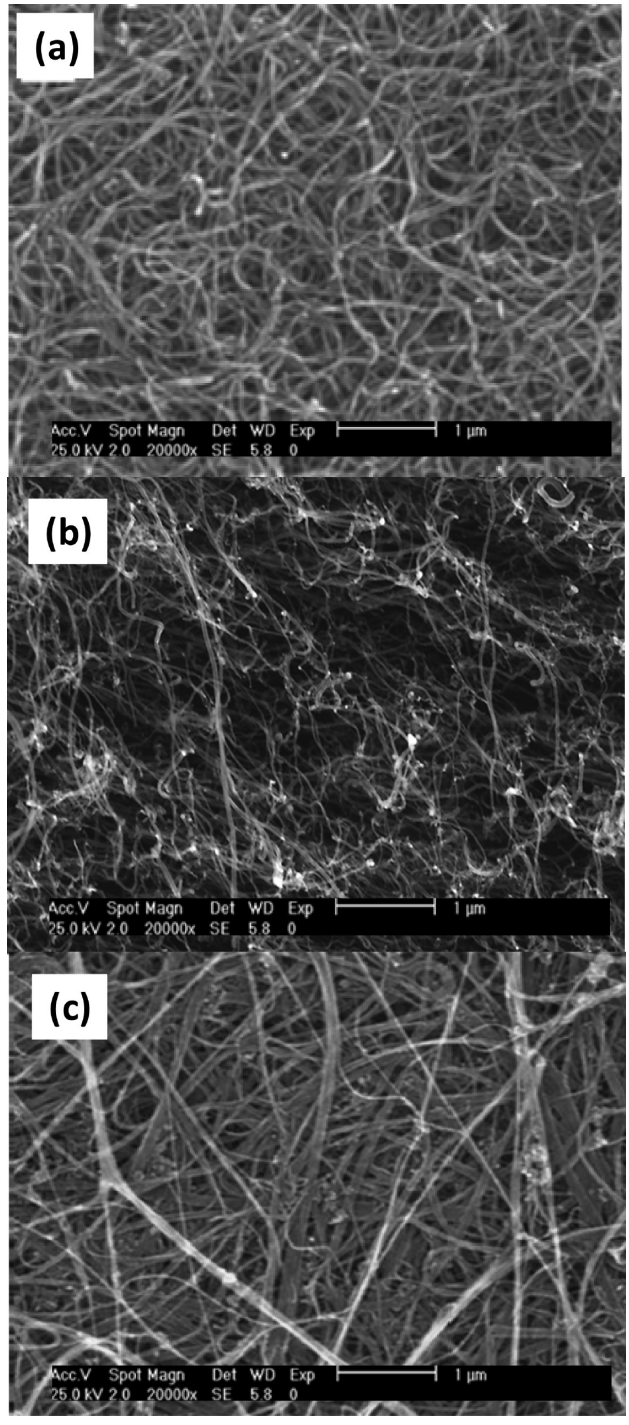

Figure 2. Typical SEM micrographs of MW3NH-BP (a), SW1-BP (b), and MW3-BP (c).

increased intensity of the D band. It is known that the ratio of the intensities of the G and D peaks gives information on the graphite degree or the lattice distortion of carbon-based materials. For SW1-BP, a very high G/D intensity ratio is observed (Table 1), indicative of the high quality of these nanotubes. BPs synthesized from MWCNTs, particularly those with functionalized nanotubes, exhibit a low G/D ratio, since the oxidation in nitric acid results in the formation of additional defects on the tube sidewalls.[26] Further, a broadening of the G band is detected for the acid and amide-functionalized BPs,

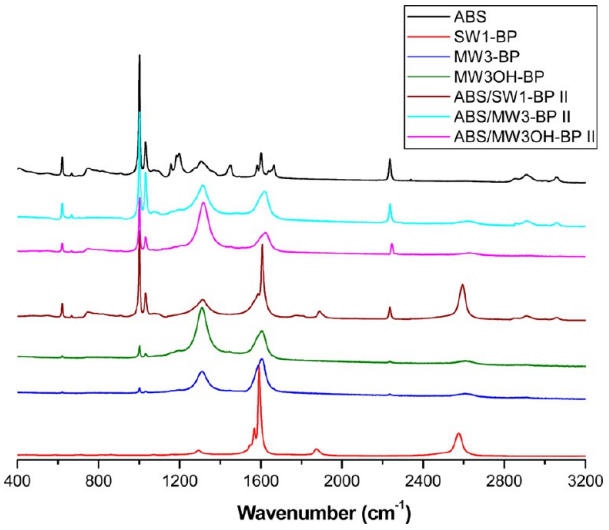

Figure 3. Room temperature Raman spectra of neat ABS, pristine, and functionalized buckypapers and the corresponding composites manufactured via vacuum infiltration.

indicating a double resonance feature due to disorder and defects.[28]

Morphological Characterization of the Nanocomposites. To assess the impregnation quality of the manufactured nanocomposites, their surface morphology was examined by SEM, and typical images of ABS/MW3OH-BP and ABS/MW3-BP are displayed in Figure 4. Very different features were observed depending on the fabrication process and the BP architecture. ABS/MW3OH-BP composite prepared via hot-compression (Figure 4a) is quite heterogeneous, showing matrix-rich regions and nonimpregnated areas. Albeit the resin wets well the CNT ropes in the periphery of the sample, there is low degree of impregnation in the central areas, as can be clearly visualized in the high-magnification image (Figure 4b). Under pressure, the matrix was forced to penetrate the BP, but due to its low permeability, the resin displaced the ropes, generating random channels through the nanotube network. The small pore size of the BP and the high viscosity of the terpolymer preclude complete tube wetting, leading to a high degree of composite porosity. Analogous images were obtained for ABS/MW3NH-BP and ABS/MW7-BP nanocomposites, related to the higher bulk density of the corresponding BP networks (Table 1). In contrast, samples prepared via resin infusion exhibited a more homogeneous BP impregnation (Figures 4c and d), since the vacuum was uniformly applied to the whole system. The nanotube bundles are surrounded by the polymer matrix, which had penetrated through the entire BP thickness during the infiltration process, resulting in better wetting, hence lower void content, and partial alignment of the CNT ropes along the polymer flow (thickness direction), particularly for BPs with functionalized tubes. Thus, in the micrograph at high magnification (Figure 4d), only a few voids were detected. In contrast, ABS/MW3-BP nanocomposites manufactured either by hot-compression (Figures 4e and f) or vacuum infiltration (images not shown) exhibited very high degree of resin impregnation and minimum level of porosity. Similar morphology was found for ABS/SW1-BP composites, ascribed to the high permeability of this type of BP that enables the diffusion of the polymer chains through the entire CNT sheet upon application of pressure or vacuum.

ABS and the nanocomposites were also characterized by Raman spectroscopy to obtain information about the BP-matrix interactions (Figure 3). Note that almost identical spectra were recorded for samples prepared by either vacuum infiltration or hot-compression, hence only representative data for class II composites are shown. The spectrum of neat ABS shows an intense band at ~2236 cm^{-1} assigned to the C≡N stretching of acrylonitrile monomer.[29] The bands centered at 1660 and 1590 cm^{-1} arise from the C═C and C−C stretching of the aromatic rings of the styrene monomer, and the peaks in the ranges of 1033−990 and 620−750 cm^{-1} are related to aromatic C−H in plane and out of plane bending, respectively. Further, a few weak signals related to CH_2 and CH_3 groups are observed: the C−H stretching in the range of 2900−3054 cm^{-1}, as well as the CH_2 bending, twisting and rocking at about 1448, 1308, and 1190 cm^{-1}, respectively. The spectrum of ABS/SW1-BP nanocomposites is quite similar to that of the neat polymer matrix, although the characteristic peaks of ABS exhibit decreased intensity. The major difference is the broad band centered at 1604 cm^{-1} that arises from the overlapping of the G band of the BP and the aromatic peak of ABS at 1590 cm^{-1}, slightly shifted to higher frequencies. The upshift of the G mode provides evidence of the ABS-SW1-BP interactions, mainly through $\pi-\pi$ stacking. The delocalization and hybridization of π electrons between CNTs and polymers containing aromatic rings, such as PS, PPS, or PEEK, has been previously reported for several BP reinforced nanocomposites,[11,18] leading to polymer adsorption onto the nanotube surface. Moreover, a wide peak appears at ~1300 cm^{-1} related to the D band of the SWCNTs that overlaps with the CH_2 twisting, and another strong signal is detected at 2600 cm^{-1} ascribed to the G′ band of the nanotubes, although shifted to higher wavenumber. This fact is again indicative of the matrix-BP interactions, and could also be ascribed to the strong compressive forces because of the presence of polymer chains onto the CNTs.[30] Composites reinforced with unfunctionalized or functionalized MWCNTs also present similar spectrum to that of neat ABS, with a broadening and upshift of the G band of the MWCNTs up to 1610 and ~1621 cm^{-1}, respectively, because of interactions between the tubes and the matrix. In addition, an intense signal is found at 1300 and ~1317 cm^{-1}, respectively, related to the D band of the MWCNTs. The upshift of the D mode is more pronounced for composites incorporating functionalized MWCNTs compared to that reinforced with the pristine counterpart, suggesting stronger polymer-BP interactions that may arise from the higher hydrophilicity of BPs with carboxylic or amide groups, which can undergo polar interactions with the nitrile groups of ABS. Further, nitriles may also act as hydrogen bond acceptors, thus forming H-bonds with the functional groups of the BPs.

Thermogravimetric Analysis. To evaluate the thermal stability of the composites and determine their average resin and void content, TGA experiments were carried out under nitrogen and dry air atmospheres. Figure 5 shows, as an example, TGA curves for neat ABS, SW1-BP, MW3NH-BP, MW3OH-BP, and the corresponding nanocomposites manufactured by either of the two methods. The degradation temperatures, composition and degree of porosity of all the composites tested are collected in Table 2. Regarding the decomposition under inert atmosphere (Figure 5a), neat ABS exhibits a single degradation stage, that initiates (T_i) at ~368 °C and shows the maximum rate of weight loss (T_{max}) around 421 °C, leading to the total decomposition of the polymer.

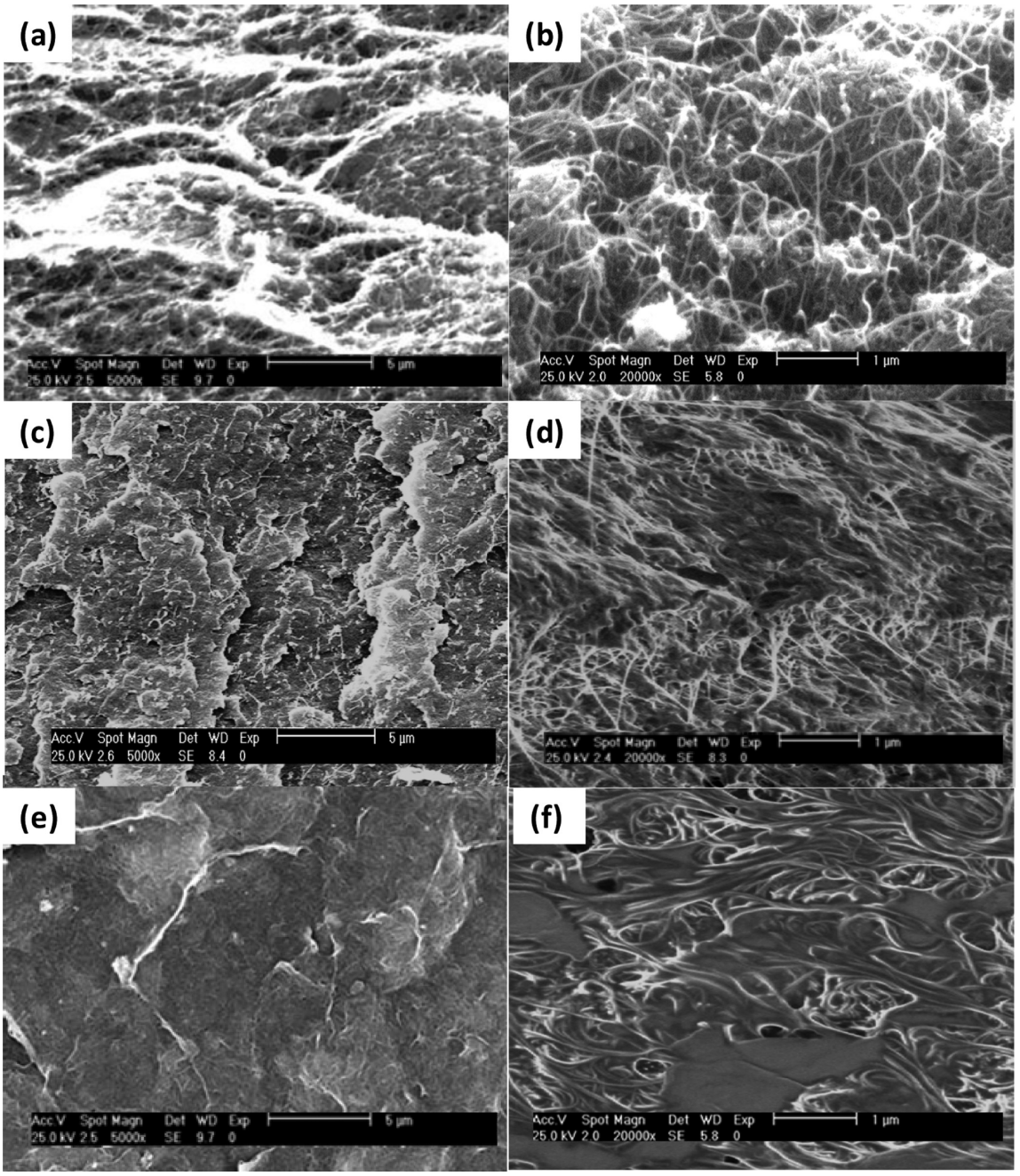

Figure 4. SEM images at different magnifications from the cross section of ABS-based nanocomposites. (a and b) ABS/MW3OH-BP I; (c and d) ABS/MW3OH-BP II; (e and f) ABS/MW3-BP I.

SW1-BP reinforced nanocomposites display analogous degradation curves to that of pure ABS albeit shifted to higher temperatures. The increments in T_i and T_{max} are on average 41 and 44 °C for samples prepared via hot-compression and vacuum infiltration, respectively. Similar behavior was observed for nanocomposites incorporating pristine or short MWCNTs, with slightly higher rises (Table 2). These significant thermal stability improvements are ascribed to the presence of the BP sheet that causes an important barrier effect, hindering the diffusion of the degradation products from the bulk of the polymer to the gas phase, hence slowing down the mass loss rate. In fact, the formation of a continuous structured network has been found to act as a protective layer that reduces the release of decomposition gases from the polymeric matrix underneath into the atmosphere.[31,32] The small differences found between the degradation temperatures of ABS/SW1-BP and ABS/MW3-BP composites (either class I or II, see Table 2) are probably related to their similar degree of matrix impregnation, as revealed by SEM images. Regarding samples incorporating functionalized MWCNTs, the degradation curves exhibit a small weight loss in the range of 200−400 °C associated to the decomposition of surface functional groups, comparable to that found in the corresponding BPs. Albeit they start to degradate somewhat earlier than the pure polymer matrix, these nanocomposites exhibit the highest T_{10} (temperature of 10% weight loss) and T_{max} values, particularly those with carboxylic groups, which display up to 56 and 65 °C T_{max} enhancements when prepared via hot-compression or vacuum

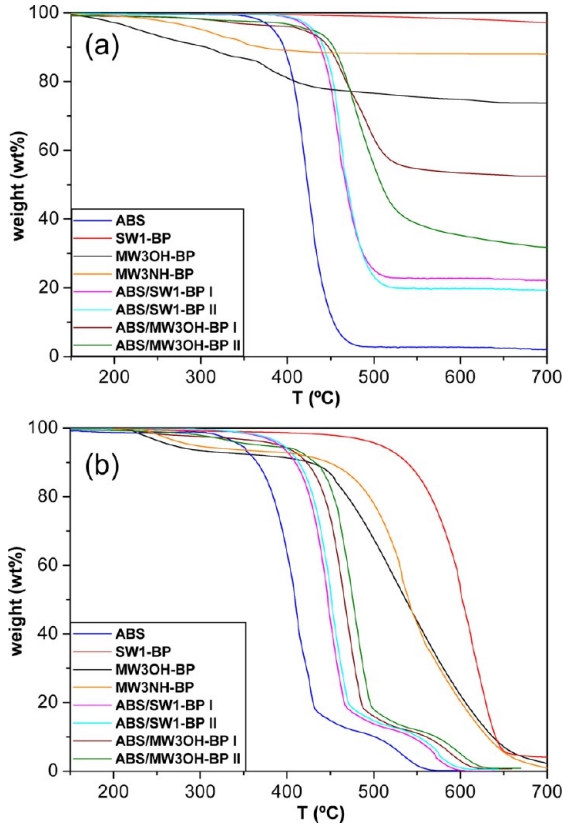

Figure 5. TGA curves for neat ABS, SW1-BP, MW3OH-BP, MW3NH-BP, and the corresponding composites under nitrogen (a) and dry air (b) atmospheres.

infiltration, respectively. Note that these increments are larger than those reported for BP-reinforced PEEK,[11] polyimide,[33] epoxy,[31] or ABS/MWCNT composites.[10] The exceptional thermal stability increases attained in this work are attributed to the high CNT purity and content of the composites combined with a very efficient barrier effect of the dense and highly entangled BP mat and strong nanotube-matrix interactions. Further, the higher degradation temperatures for samples prepared via resin infusion probably arise from their improved matrix wetting. Focusing on the degradation under oxidative environment (Figure 5b), qualitatively similar trends were observed, with larger thermal enhancements for samples reinforced with more compact BP networks (Table 2). In this case, neat ABS and the composites reinforced with pristine BPs show two degradation stages, while those with functionalized tubes display three stages, the first again arising from the decomposition of surface functional groups.

To estimate the weight fraction of polymer matrix (w_m) within the composites, the following equation was applied:[11] $w_m = [m_b - m_c + w_i(1 - m_b)]/(m_b - m_m)$, where m_b, m_m, and m_c are the weight residue of buckypaper, polymer matrix and composite under inert atmosphere, respectively, and w_i is the weight content of impurities (Table 1). The results obtained for the different composites are collected in Table 2. ABS/SW1-BP exhibits the highest w_m, about 80% when fabricated via vacuum infiltration, consistent with the larger pore size of the loose BP network that facilitates the penetration of the matrix chains. For this type of BP, small differences are found between w_m of composites prepared by either of the two techniques, since almost total impregnation is attained by both methods, in agreement with SEM analysis. In contrast, ABS/MW3OH-BP presents the lowest w_m, particularly when manufactured by hot-compression (~30%), related to the smaller pore diameter of the compact and entangled BP mat that prevents complete matrix wetting, as mentioned earlier. Low w_m values were also estimated for composites with amide-functionalized MWCNTs (Table 2). The theoretical density (ρ_T) of the composites was calculated according to the expression:[11] $\rho_T = 100/[(w_m/\rho_m) + (w_f/\rho_f)]$, where w_f is the weight percentage of CNTs and ρ_m and ρ_f are the density of the matrix and filler, respectively. The void content was determined as difference between the experimental and the theoretical density: v_c (%) = $[(\rho_T - \rho_c)/\rho_T] \times 100$. As expected, composites with functionalized MWCNTs display the highest v_c (up to ~15%), while those incorporating pristine CNTs present low degree of porosity (1–5%, Table 2). This is a crucial parameter that greatly influences the mechanical performance of the materials.

Thermal Conductivity. Figure 6 shows the room temperature thermal conductivity (λ) for the different BPs and the corresponding nanocomposites. Regarding the BPs, the

Table 2. Characteristic Degradation Temperatures, Matrix Weight Fraction, and Void Content for the Different ABS Nanocomposites Obtained from TGA Measurements under Nitrogen and Dry Air Atmospheres[a]

	inert atmosphere					oxidative atmosphere			
sample	T_i (°C)	T_{10} (°C)	T_{max} (°C)	w_m (%)	v_c (%)	T_i (°C)	T_{10} (°C)	T_{maxI} (°C)	T_{maxII} (°C)
ABS	368 ± 1	396 ± 1	421 ± 2			318 ± 1	365 ± 1	411 ± 2	522 ± 2
ABS/MW3-BP I	411 ± 1	438 ± 2	464 ± 1	67.5 ± 0.6	4.4 ± 0.7	364 ± 2	410 ± 1	449 ± 2	560 ± 1
ABS/MW7-BP I	415 ± 2	440 ± 1	468 ± 2	54.4 ± 0.4	8.3 ± 1.1	368 ± 1	413 ± 1	456 ± 3	566 ± 2
ABS/SW1-BP I	409 ± 1	436 ± 1	462 ± 1	76.6 ± 0.7	2.5 ± 0.3	361 ± 2	408 ± 2	448 ± 1	561 ± 2
ABS/MW3OH-BP I	317 ± 1	448 ± 1	477 ± 3	29.8 ± 0.3	15.1 ± 1.9	299 ± 1	422 ± 1	466 ± 2	575 ± 3
ABS/MW3NH-BP I	323 ± 2	445 ± 2	470 ± 1	34.3 ± 0.4	13.6 ± 2.0	302 ± 2	419 ± 2	460 ± 1	570 ± 2
ABS/MW3-BP II	414 ± 2	443 ± 2	467 ± 1	74.2 ± 0.6	2.9 ± 0.3	366 ± 1	418 ± 1	455 ± 3	562 ± 2
ABS/MW7-BP II	419 ± 1	447 ± 2	472 ± 1	66.9 ± 0.7	4.6 ± 0.6	373 ± 1	424 ± 2	459 ± 1	569 ± 1
ABS/SW1-BP II	412 ± 2	441 ± 1	465 ± 2	80.1 ± 0.8	1.2 ± 0.2	362 ± 1	416 ± 2	452 ± 1	565 ± 2
ABS/MW3OH-BP II	326 ± 1	460 ± 2	486 ± 1	55.8 ± 0.5	8.0 ± 1.0	305 ± 1	433 ± 1	476 ± 2	581 ± 1
ABS/MW3NH-BP II	328 ± 1	453 ± 1	481 ± 3	58.7 ± 0.6	6.8 ± 0.8	307 ± 2	427 ± 2	470 ± 1	577 ± 3

[a]Composites manufactured via hot-compression or vacuum infiltration are designated as class I and II, respectively. For comparison, data of neat ABS are also tabulated. T_i = initial degradation temperature obtained at 2% weight loss; T_{10} = temperature corresponding to 10% weight loss; T_{max} = temperature of maximum degradation rate; w_m = matrix weight fraction; v_c = void content. The subscripts I and II refer to the first and second degradation stages under oxidative atmosphere.

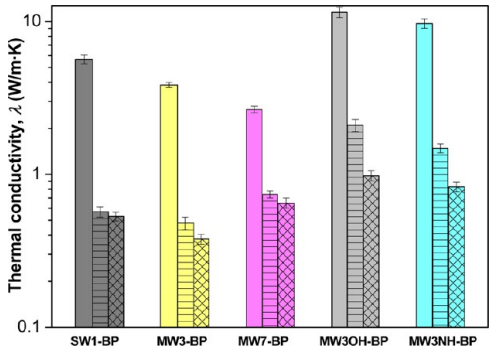

Figure 6. Room temperature thermal conductivity for the different BPs (□) and the corresponding composites manufactured via vacuum infiltration (≡) or hot-compression (×).

magnitude of λ is strongly dependent on their density, CNT characteristics (size, chirality, degree of entanglement, alignment, purity, defects, and so forth) and the resistance due to tube−tube junctions (interfacial thermal resistance between nanotubes).[34,35] Previous works revealed λ data between 50 and 200 W/mK for magnetically aligned BPs, where the nanotubes are tightly packed and oriented in-plane,[36] whereas values in the range of 2−30 W/mK have been reported for randomly oriented BPs.[34] Among the BPs synthesized in this work, MW7-BP displays the lowest λ (~2.7 W/mK), since short CNTs lead to more contact barriers between tubes, hence reduced conductivity. In addition, the metal catalyst impurities embedded in the BPs increase the scattering during phonon transfer. SW1-BP and MW3-BP show intermediate values (~5.7 and 3.8 W/mK, respectively), since they are loose CNT networks that contain a large number of macropores filled with air ($\lambda \approx 0.026$ W/mK), as revealed by SEM micrographs (Figure 2), and when the heat is transmitted from the CNTs to the air results in natural convection of air in the macropores, reducing the heat transfer to the rest of the sample. BPs with functionalized MWCNTs exhibit the highest λ values (~11.5 W/mK for MW3OH-BP), related to the denser mat and the higher nanotube purity, since metal catalysts and carbonaceous impurities have been reported to impair the nanotube thermal conductivity.[35] Nevertheless, the values attained are far from the experimental measurements on a single MWCNT[37] (~3000 W/mK) or SWCNT[38] (~6000 W/mK), because of the high interfacial thermal resistance between CNTs.

Neat ABS presents a low thermal conductivity (~0.17 W/mK), which improves by about 12-fold and 8-fold upon impregnation of MW3OH-BP and MW3NH-BP, respectively, via vacuum infiltration. These significant enhancements are consistent with results reported for epoxy composites reinforced with acid-treated nanotubes,[39] where the purification treatment strongly increased the conductivity of the composites due to their higher effective CNT concentration, and confirms that the thermal conduction is nanotube dominated. Further, these composites exhibit a partial degree of CNT alignment induced during processing, as revealed by SEM (Figure 4), which is known to increase the conductivity.[36] In addition, the functionalization improves the CNT-matrix interfacial bonding, thus reducing the phonon scattering between the two phases.[39] However, considerably smaller increments are found for composites prepared via hot-compression (around 6 and 5 fold enhancements for the aforementioned BPs), since this procedure results in random tube alignment and uneven matrix wetting. Regarding samples incorporating pristine CNTs, the increments are between two and 4-fold, being larger for those incorporating shorter nanotubes probably because of their higher CNT content. In these composites, the processing method has less influence on the conductivity, in agreement with the high and similar degree of impregnation attained by the two techniques.

Electrical Conductivity. The room temperature DC electrical conductivity (σ) of the BPs and the composites is shown in Figure 7. As can be observed, the BPs exhibit σ values

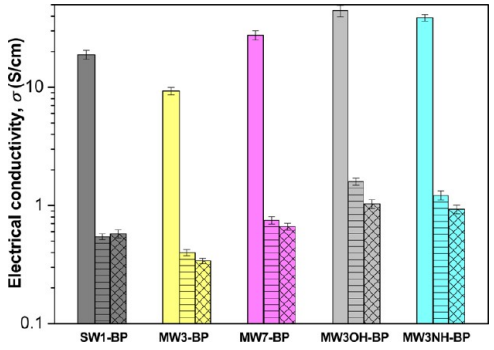

Figure 7. DC electrical conductivity of the different BPs and the corresponding composites: BPs (□), vacuum infiltration (≡), or hot-compression (×).

in the range of 9−45 S/cm, consistent with previously reported literature data.[15,21] Interestingly, the acid and amide-functionalized buckypapers exhibit the highest electrical conductivity. To understand this behavior, the mechanism of electrical conduction within a CNT film has to be considered. According to the variable-range hopping (VRH) theory,[40] the BP is a 3D network of dispersed bundle−bundle junctions, and the electrical conduction occurs either tube−tube within a bundle or between neighbor bundles through their contacts. Therefore, σ depends essentially on two factors, the conductivity of the nanotubes themselves and the ability of the electric carriers to tunnel between adjacent nanotubes. Regarding the first factor, it was found that the acid treatment induced some defects on the CNT sidewalls, as revealed by the Raman spectra, which might have modified the conjugation system for electron transport, resulting in a slight decrease in σ. On the other hand, chemical modification treatments are reported to enhance the CNT interactions, charge carrying and transport capabilities.[41] Additional charge carriers in the form of either p-type or n-type doping can be developed after acid treatment,[42] which can also convert semiconducting nanotubes into metallic tubes by altering their Fermi level, leading to an increase of intrinsic conductivity and a decrease of resistance because of semiconducting-metallic junctions through mitigation of the Schottky barrier.[43] Thus, the disadvantages of the functionalization with respect to the nanotube conductivity seem to be outweighed by the improved transport capability due to the stronger interactions between neighbor tubes, and the overall result is an increase in electrical conductivity. Further, as the network density increases, more conductive pathways for the charge carriers are available, yielding an increase in conduction within the film. The above-mentioned facts explain the high conductivity of MW3OH-BP and MW3NH-BP which have very dense structures, and also that MW7-BP exhibits higher σ than MW3-BP (Figure 7), since shorter tubes result in a more compact arrangement. Interestingly, SW1-BP shows improved σ compared to MW3-BP, despite its higher void content,

probably related to the higher conductivity of this type of nanotubes, in agreement with previous works.[44]

Neat ABS is electrically insulating ($\sigma \approx 10^{-12}$ S/cm),[10] and its conductivity increased by more than eleven orders of magnitude upon BP impregnation. Nevertheless, the composites show σ values between 18-fold and fifty 5-fold lower than those of the corresponding BPs, because the nanotubes are coated by a thin layer of insulating polymer that acts as a barrier to tube−tube hopping. Analogous behavior has been reported for different BP-reinforced polymers.[12,21,45] As expected, the trends observed for σ of the composites are qualitatively similar to those described above for the BPs, and ABS/MW3OH-BP shows the highest σ value, attributed to its denser CNT film and lower resin content, given that the electrical resistance nanotube-matrix is considerably stronger than between CNTs. However, differences among σ of the composites are smaller than those between the BP counterparts. On the other hand, slight variations are observed between data of composites prepared by either of the two techniques, because of their different CNT content and extent of nanotube wetting.

It is important to highlight that the improvements in the electrical conductivity of ABS attained upon BP impregnation are on average 2 orders of magnitude higher than those reported for the addition of MWCNTs[10] or CB.[7] Overall, our results demonstrate the effectiveness of the dense and small pore size BPs to improve the electrical and thermal properties of ABS for electronic applications. All the developed composites exhibit an electrical conductivity higher than 0.3 S/cm, hence they are well suitable for packaging of integrated circuit devices, where electrostatic charge dissipation is required.[6] Further, those incorporating functionalized BPs show σ values ≥1 S/cm, therefore they show great potential as EMI shielding materials.[1]

Dynamic Mechanical Analysis. The viscoelastic properties (storage modulus, loss modulus and damping ratio) were measured by DMA, a technique that provides valuable insights into the stiffness of the materials as well as the molecular relaxations taking place as a function of temperature. Figure 8 shows typical storage modulus (E′) and loss tangent (tan δ) vs temperature curves at the frequency of 1 Hz for neat ABS, MW3-BP, MW3OH-BP, and the corresponding composites. DMA data for all the samples are collected in Table 3. The modulus of the BPs hardly changes with temperature, being considerably higher for those with functionalized CNTs (∼4.1 GPa) compared to those comprising pristine MWCNTs (∼0.9 GPa) or SWCNTs (∼1.5 GPa). This behavior is related to the increased bulk density, hence larger number of interconnections in the former BPs, and the fact that SWCNTs display higher stiffness than MWCNTs.[46] E' of neat ABS drops progressively with temperature, showing a strong decay in the vicinity of the glass transition (close to 113 °C). At 25 °C, the modulus of ABS is 1.7 GPa, and increases by about 140 and 130% for composites reinforced with SW1-BP and MW3-BP, respectively, prepared via vacuum infiltration, indicating the high stiffening effect of the CNT mat. These strong enhancements, considerably larger than those reported for ABS/MWCNT nanocomposites,[10] are ascribed to the uniform matrix wetting and low void content of these samples. In the case of composites prepared via hot-compression, the increments are slightly smaller, ∼120 and 88%, respectively. Qualitatively analogous behavior of E' improvement was reported for BP-reinforced epoxy composites.[20] In contrast, samples incorporating functionalized MWCNTs prepared via

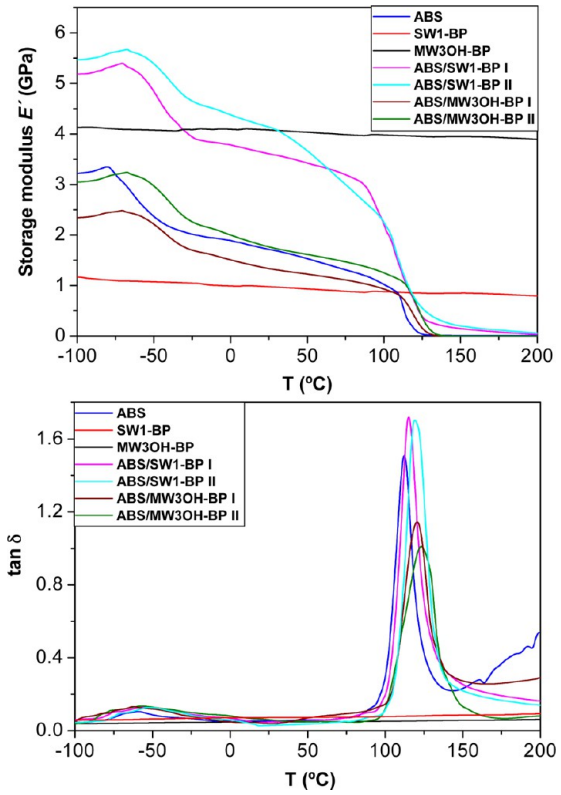

Figure 8. Storage modulus E' (top) and tan δ (bottom) as a function of temperature for neat ABS, SW1-BP, MW3OH-BP, and the corresponding composites.

vacuum infiltration or hot-compression display similar or even lower E' than the matrix, respectively, related to their high degree of porosity (Table 2), factor that is known to have an important detrimental effect on the composite mechanical performance. Analogously, only a small E' increment (∼18%) was obtained upon impregnation of short MWCNTs via hot-compression, due to the relatively high composite void content, while a moderate increase of 58% was found when they were prepared via vacuum infiltration. As the temperature rises, E' of all the polymeric samples diminishes, showing a strong drop around the glass transition, where the polymer chains become more mobile and lose their close packing arrangement. In the rubbery region, the differences in modulus between the composites and the neat polymer are slightly less marked; for instance, at 100 °C, ABS/MW3-BP composites (class I and II) show ∼100 and 70% higher E' than the pure polymer matrix, respectively (Table 3), indicating that the stiffening effect is more pronounced below the softening point of the resin.

The evolution of the damping factor or tan δ (ratio of the loss to storage modulus) as a function of temperature is shown in the lower part of Figure 8. Neat ABS displays two relaxation peaks,[47] one around −58 °C with small tan δ magnitude, assigned to the glass transition of polybutadiene ($T_{g,I}$), and other very intense at ∼113 °C related to the glass transition of polystyrene-co-acrylonitrile ($T_{g,II}$). The same relaxations are observed for the composites, albeit in general shifted to higher temperatures (Table 3), since the BP network restricts the mobility of the polymer chains. The largest increments are found for samples with functionalized MWCNTs; in particular ABS/MW3OH-BP prepared via vacuum infiltration shows ∼10 °C higher $T_{g,II}$ than pure ABS, ascribed to its stronger filler−

Table 3. DMA Data for Neat ABS and the Different BP-Reinforced Composites[a]

sample	$T_{g,I}$ (°C)	$T_{g,II}$ (°C)	$E'_{-100°C}$ (GPa)	$E'_{25°C}$ (GPa)	$E'_{100°C}$ (GPa)	tan δ_{max} (a.u.)	fwhm (°C)	tan δ_{area} (a.u.)
ABS	−58 ± 1	113 ± 1	3.2 ± 0.2	1.7 ± 0.1	1.0 ± 0.1	1.46 ± 0.05	14.1 ± 1.0	24.0 ± 3.1
ABS/MW3-BP I	−57 ± 1	115 ± 1	4.7 ± 0.2	3.2 ± 0.2	1.7 ± 0.1	1.58 ± 0.06	14.5 ± 1.2	25.2 ± 3.0
ABS/MW7-BP I	−60 ± 2	112 ± 1	3.5 ± 0.1	2.0 ± 0.1	1.4 ± 0.1	1.47 ± 0.05	12.9 ± 1.1	22.3 ± 2.9
ABS/SW1-BP I	−55 ± 1	116 ± 2	5.2 ± 0.3	3.8 ± 0.2	2.2 ± 0.2	1.64 ± 0.07	15.0 ± 1.2	27.1 ± 3.2
ABS/MW3OH-BP I	−56 ± 2	120 ± 2	2.4 ± 0.1	1.3 ± 0.1	0.9 ± 0.1	1.10 ± 0.04	17.5 ± 1.3	21.7 ± 2.7
ABS/MW3NH-BP I	−50 ± 1	117 ± 1	2.8 ± 0.1	1.5 ± 0.1	1.0 ± 0.1	1.15 ± 0.04	16.4 ± 1.4	21.4 ± 2.6
ABS/MW3-BP II	−54 ± 1	119 ± 1	4.9 ± 0.2	3.9 ± 0.2	2.0 ± 0.1	1.57 ± 0.06	14.2 ± 1.2	24.8 ± 3.0
ABS/MW7-BP II	−55 ± 2	118 ± 1	3.9 ± 0.2	2.7 ± 0.1	1.5 ± 0.1	1.45 ± 0.05	13.3 ± 1.2	23.0 ± 2.8
ABS/SW1-BP II	−49 ± 1	119 ± 1	5.5 ± 0.3	4.1 ± 0.2	2.2 ± 0.2	1.62 ± 0.07	16.1 ± 1.4	28.9 ± 3.2
ABS/MW3OH-BP II	−53 ± 2	123 ± 2	3.0 ± 0.1	1.8 ± 0.1	1.2 ± 0.1	1.01 ± 0.04	20.2 ± 1.6	23.2 ± 2.8
ABS/MW3NH-BP II	−52 ± 2	121 ± 1	3.1 ± 0.2	2.1 ± 0.1	1.3 ± 0.1	1.08 ± 0.04	18.5 ± 1.5	22.4 ± 2.6

[a] T_g = glass transition temperature (the subscripts I and II refer to the T_g of polybutadiene and polystyrene-co-acrylonitrile phases, respectively); E' = storage modulus; tan δ_{max} = maximum of tan δ peak; fwhm = full width at half-maximum of tan δ peak; tan δ_{area} = area under tan δ peak.

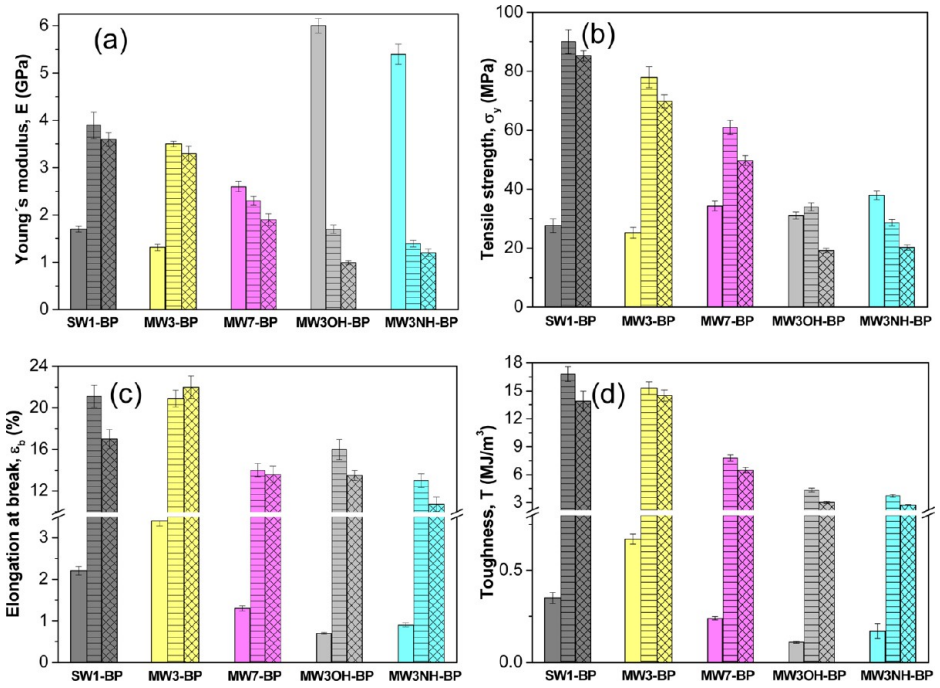

Figure 9. Young's modulus E (a), tensile strength σ_y (b), elongation at break ε_b (c), and toughness T (d) obtained from the stress−strain curves of the different samples. Symbols as indicated in Figure 6

matrix interactions, as revealed by the Raman spectra (Figure 3), since the T_g is very sensitive to interfacial interactions between the polymer and the reinforcements; it could also be related with the higher CNT content of this sample. Smaller increments (around 5−6 °C) are found for composites incorporating pristine CNTs, while those with short MWCNTs show approximately the same $T_{g,II}$ as neat ABS. Similar trends are found for $T_{g,I}$ values, albeit the differences compared to that of the pure polymer are smaller. Note that the increments in T_g attained in this work are considerably larger than those observed for bulk ABS/MWCNT composites,[10] hinting toward the more effective immobilization ability caused by the dense MWCNT mat. It can also be observed from Figure 8 that the height of tan δ peak for the composites with amide and acid-functionalized MWCNTs is considerably lower than that of the neat polymer, indicative of higher ratio of the stored to loss energy in the zone of the T_g. This decrease in tan δ_{max} value should be related to the strong hindrance to chain mobility imposed by the dense and entangled CNT networks; the diminution in height is more pronounced for class II composites, probably related to their lower void content. However, composites incorporating pristine CNTs exhibit similar or even higher tan δ_{max} than neat ABS (Table 3), suggesting weaker nanofiller−matrix interfacial interactions, as revealed by the Raman spectra. On the other hand, most of the composites display wider tan δ peak than the neat polymer, which may be due to the confinement of polymer segments within the nanotube networks; the CNTs disturb the relaxation of neighboring polymer chains, leading to longer relaxation times that is reflected in a broadening of the peak. The data for full width at half-maximum (fwhm) are also collected in Table 3. The largest broadening (around 6 °C) is observed for ABS/MW3OH-BP II, and should also arise from the enhanced filler−matrix interactions. An analogous effect has been previously reported for other BP-reinforced polymers,[20,21] attributed to a less homogeneous amorphous phase in the composites compared to that of the neat polymer. Another important parameter that can be derived from the damping

curves is the area under tan δ peak, since it is indicative of the energy dissipated in viscoelastic relaxations. Any molecular process that promotes energy dissipation would enhance the impact resistance of polymeric systems, as was underlined by Kausch's statement.[48] Interestingly, ABS/SW1-BP II exhibits the highest value, suggesting improved ability of this material to absorb energy during the deformation process, thereby better impact resistance. In contrast, composites with a large number of interconnections between the CNTs display smaller area than the bare resin, since their dense CNT network cannot undergo viscoeleastic deformation.

Static Mechanical Properties. Further characterization of the mechanical properties was carried out by tensile tests. The average Young's modulus (E), tensile strength (σ_y), elongation at break (ε_b), and toughness (T) obtained from the stress−strain curves of the different samples investigated are displayed in Figure 9. Regarding the mechanical properties of BPs, a variety of data for σ_y (2−80 MPa) and E (0.5−15 GPa) have been published in the literature.[13,18,21,42,49,50] The disparity in the measured values arises from the large number of parameters affecting their mechanical performance such as CNT length, type, chemical treatment, alignment, void content, and so forth. Pristine BPs show the lowest E and σ_y albeit the highest ε_b, due to the low energy required to debridge the CNTs during the tensile deformation as a result of their loose structure and weak van der Waal forces between the nanotubes. Despite its higher void content, E of SW1-BP is slightly higher than that of MW3-BP, in agreement with DMA, albeit both types of sheets display similar σ_y. On the other hand, BPs comprising short MWCNTs show higher stiffness and strength albeit reduced ductility than samples made of the long counterparts, consistent with their increased density. More importantly, the stiffest films are those incorporating functionalized MWCNTs, attributed to their larger number of tube interconnections that result in better structural integrity; they also exhibit slightly higher tensile strength although lower ductility than composites with pristine BPs, since the strong interactions between the tubes hinder the plastic deformation of the material. Regarding the toughness measured as the area under the tensile curve, MW3-BP presents the highest value while the acid-functionalized counterpart is the most brittle film, related to their extent of ductile deformation.

E of neat ABS is about 1.6 GPa, and increases between 19% and 145% upon impregnation with pristine BPs (Figure 9a); the largest increment is found for ABS/SW1-BP II, suggesting very effective stress transfer ability from the matrix to the SWCNT network. However, the stiffness of the polymer hardly increases or even decreases slightly when reinforced with functionalized BPs, in good agreement with the results from DMA tests. As mentioned previously, the extent of modulus improvement is strongly influenced by the impregnation degree, void content, CNT concentration as well as nanofiller−matrix interfacial interactions. Despite the fact that ABS/MW3OH-BP exhibits stronger nanotube-matrix interactions than composites with raw MWCNTs, as evidenced by the Raman spectra (Figure 3), and possesses higher CNT content, it shows lower or comparable modulus than that of the neat polymer when manufactured via hot-compression or vacuum infiltration, respectively, behavior that can be explained considering the high void content of these composites. Thus, class I composites with less uniform BP impregnation display lower E values than the class II counterparts. Qualitatively similar trends are found for the tensile strength (Figure 9b), which is around 44 MPa for the neat polymer and increases in the range of 14−105% for composites incorporating pristine BPs, while for those with acid or amide-functionalized MWCNTs σ_y considerably decreases. It is worth noting that the improvements in stiffness and strength observed here are significantly higher than those reported for ABS/MWCNT nanocomposites incorporating interfacial modifiers,[8] demonstrating the suitability and effectiveness of our approach to produce composites for use in specific structural components. These enhancements in mechanical properties are also higher than those found for BP-reinforced PEEK or PPS,[21] and comparable to those reported for PC/BP[12] and PVA/BP composites.[18]

The experimental Young's moduli can be compared to the predictions calculated through the modified rule of mixtures described by Krenchel as[51] $E_c = (\eta_o \eta_l E_f - E_m)V_f + E_m$, where E_c, E_f, and E_m are the tensile modulus of the composite, filler, and matrix, respectively, V_f the filler volume fraction, η_o is the orientation factor (1/5 for randomly oriented fillers), and η_l is the length efficiency factor that accounts for the waviness of the fillers, assumed to be 0.27.[52] Taking E_f reported for SWCNT bundles[53] (∼300 GPa), the estimated modulus for ABS/SW1-BP was 4.4 GPa, about 22% and 13% higher than the measured values for composites I and II, respectively. The gap between the experimental and theoretical data probably arises from the presence of internal voids, as determined form TGA measurements, the shear slippage of individual nanotubes within a bundle that limits the stress transfer, the amorphous carbon and metal catalyst residues within the BP that might cause a reduction of their effective Young's modulus and the fact that the model assumes perfect filler−matrix bonding.

Regarding the elongation at break (Figure 9c), all the composites display lower value than that of neat ABS (∼31%), since the nanofillers restrict the plastic deformation of the matrix, in agreement with the behavior reported for other BP/polymer composites.[18,21] The largest decrease (∼65%) is found for ABS/MW3NH-BP I, attributed to its high MWCNT content, the strong filler−matrix interfacial interactions and the presence of a dense and entangled nanotube network that strongly obstructs the ductile flow of the polymer chains. In contrast, ε_b only drops by around 29% for ABS/MW3-BP I, consistent with the loose structure of its reinforcing network. The toughness of neat ABS is around 10.8 MJ/m^3, and increases significantly upon impregnation of BPs composed of pristine long CNTs, by up to 42% for ABS/MW3-BP II composite (Figure 9d). In contrast, samples reinforced with short or functionalized MWCNTs display lower toughness than the pure polymer, the largest decrement being ∼75% for ABS/MW3NH-BP I. This diminishing effect of the nanofillers on the toughness is consistent with the reduction in the extent of plastic deformation of the matrix and the high composite void content, since the internal pores can act as stress concentration sites under load, nucleating cracks and leading to premature failure, consequently aggravating the brittleness of the material. Systematically, the diminution in toughness is more pronounced for composites fabricated by hot-press processing, in agreement with their higher degree of porosity.

The impact resistance and dynamic mechanical properties can be correlated in terms of the area under tan δ peaks.[48] As can be observed, toughness data of the composites show qualitatively similar trend to that found for the area under DMA peaks; the results provided by both techniques indicate that very dense and entangled CNT networks decrease the

ability of the matrix to absorb energy during the deformation process, causing a detriment in the impact resistance of the polymer, while loose BP films with large pore size significantly enhance the impact properties of ABS. Overall, mechanical tests indicate that in order to fully exploit the reinforcement effect of the CNT films, these should have low bulk density with large-sized pores to allow complete matrix impregnation, minimizing the composite porosity. This result is highly significant because it demonstrates that with the proper choice of BP, the stiffness, strength and toughness of the polymer can be simultaneously improved.

4. CONCLUSIONS

The degree of porosity, morphology, thermal stability, mechanical performance, thermal and electrical conductivity of ABS-based nanocomposites reinforced with either pristine or functionalized SWCNT or MWCNT buckypapers have been characterized. The composites were prepared following two different techniques: hot-press processing and vacuum infiltration. The second procedure resulted in a more uniform BP impregnation, hence composites with lower void content. BPs made from pristine CNTs form loose networks with large pores that facilitate the penetration of the polymer, leading to nanocomposites with low degree of porosity and improved mechanical performance (i.e., higher storage modulus, Young's modulus, tensile strength and toughness). In contrast, functionalized or short MWCNTs give rise to compact mats that are more difficult to be impregnated by the matrix, resulting in composites with higher void content albeit better thermal and electrical properties due to increased number of conductive pathways and stronger filler−matrix interfacial bonding. Thus, the Raman spectra of composites with acid- and amide-functionalized MWCNTs showed a noticeable shift of the G and D bands toward the high-frequency region compared to those of the corresponding BPs, corroborating the existence of intensive $\pi-\pi$ stacking and H-bonding interactions. TGA demonstrated significant increases in the degradation temperatures of the polymer upon incorporation of the BPs, ascribed to the barrier effect of the CNTs that hinder the diffusion of volatile products from the bulk to the gas phase. The highest thermal stability and glass transition temperature were found for the composite filled with acid-functionalized MWCNTs, attributed to its higher nanotube content, high CNT purity along with a more efficient barrier effect of the highly dense and entangled nanotube mat. Results demonstrate that the final properties of these materials can be tailored by controlling the BP architecture. This study provides simple approaches to manufacture ABS nanocomposites incorporating high CNT loadings with improved thermoelectrical properties for use in electronic applications such as packing of integrated circuits; moreover, those filled with functionalized BPs show great potential as EMI shielding materials.

AUTHOR INFORMATION

Corresponding Author

*E-mail: adiez@ictp.csic.es.

Notes

The authors declare no competing financial interest.

ACKNOWLEDGMENTS

Financial support from the Ministerio de Ciencia e Innovación (MICINN, Project MAT2010-21070-C02-01) is gratefully acknowledged. A.D. would like to thank the Consejo Superior de Investigaciones Científicas (CSIC) for a JAE postdoctoral contract cofinanced by the EU.

REFERENCES

(1) Chung, D. D. L. In *Composite Materials: Functional Materials for Modern Technologies*, Engineering Materials and Processes Book Series; Springer: London, 2003.
(2) Salamone, J. C. In *Concise Polymeric Materials Encyclopedia*; CRC Press: Boca Raton, FL, 1999.
(3) Majumdar, B.; Keskkula, H.; Paul, D. *Polymer* **1994**, *35*, 3164−3172.
(4) Hage, E.; Ferreira, L.; Manrich, S.; Pessan, L. *J. Appl. Polym. Sci.* **1999**, *71*, 423−430.
(5) Greco, R.; Sorrentino, A. *Adv. Polym. Technol.* **1994**, *13*, 249−258.
(6) Pecht, M.; Agarwal, R.; McCluskey, F. P.; Dishongh, T. J.; Javadpour, S.; Mahajan, R. In *Electronic Packaging Materials and Their Properties*; Taylor & Francis: New York, 1998.
(7) Oua, R.; Gerhardta, R. A.; Marrett, C.; Moulart, A.; Colton, J. S. *Composites, Part B* **2003**, *34*, 607−614.
(8) Kuan, C.-F.; Lin, K.-C.; Chiang, C.-L.; Chen, C.-H.; Peng, H.-C.; Kuan, H.-C. *Adv. Sci. Lett.* **2013**, *19*, 559−561.
(9) Wang, W.; Luo, G.; Wei, F.; Luo, J. *J. Polym. Eng. Sci.* **2009**, *49*, 2144−2149.
(10) Singh, B. K.; Kar, P.; Shrivastava, N. K.; Banerjee, S.; Khatua, B. B. *J. Appl. Polym. Sci.* **2012**, *124*, 3165−3174.
(11) Diez-Pascual, A. M.; Guan, J. W.; Simard, B.; Gomez-Fatou, M. A. *Composites, Part A* **2012**, *43*, 997−1006.
(12) Wang, S.; Liang, Z.; Pham, G.; Park, Y. B.; Wang, B.; Zhang, C.; Kramer, L.; Funchess, P. *Nanotechnology* **2007**, *18*, 1−6.
(13) Kastanis, D.; Tasis, D.; Papagelis, K.; Parthertios, J.; Tsakiroglou, C.; Galiotis, C. *Adv. Compos. Lett.* **2007**, *16*, 243−248.
(14) Whitby, R. L. D.; Fukuda, T.; Maekawa, T.; James, S. L.; Mikhalovsky, S. V. *Carbon* **2008**, *46*, 949−956.
(15) Park, J. G.; Smithyman, J.; Lin, C. Y.; Cooke, A.; Kismarahardja, A. W.; Li, S.; Liang, R.; Brooks, J. S.; Zhang, C.; Wang, B. *J. Appl. Phys.* **2009**, *106*, 104310−104316.
(16) Boge, J.; Sweetman, L. J.; in het Panhuis, M.; Ralph, S. F. *J. Mater. Chem.* **2009**, *19*, 9131−9140.
(17) Lahiff, E.; Leahy, R.; Coleman, J. N.; Blau, W. J. *Carbon* **2006**, *44*, 1525−1529.
(18) Coleman, J. N.; Blau, W. J.; Dalton, A. B.; Munoz, E.; Collins, S.; Kim, B. G. *Appl. Phys. Lett.* **2003**, *82*, 1682−1684.
(19) Frizzell, C. J.; in het Panhuis, M.; Coutinho, D. H.; Balkus, K. J.; Minett, A. I.; Blau, W. J.; Coleman, J. N. *Phys. Rev. B* **2005**, *72*, 245420−245428.
(20) Lopes, P. E.; van Hattum, F.; Pereira, C. M. C.; Novoa, P. J. R. O.; Forero, S.; Hepp, F.; Pambaguian, L. *Compos. Struct.* **2010**, *92*, 1291−1298.
(21) Diez-Pascual, A. M.; Guan, J. W.; Simard, B.; Gomez-Fatou, M. A. *Composites, Part A* **2012**, *43*, 1007−1015.
(22) Diez-Pascual, A. M.; Naffakh, M. *Carbon* **2012**, *50*, 857−868.
(23) Clark, L. M.; Taylor, R. E. *J. Appl. Phys.* **1975**, *46*, 714−719.
(24) Wu, C.-H. In Chemical Vapor Deposition of Carbon Nanostructures and Carbon Nanotubes-Reinforced Composites. Ph.D. thesis, University of Rochester, New York, 2006.
(25) Kukovecz, A.; Smajda, R.; Konya, Z.; Kiricsi, I. *Carbon* **2007**, *45*, 1696−1716.
(26) Díez-Pascual, A. M.; Naffakh, M.; Gómez, M. A.; Marco, C.; Ellis, G.; Martinez, M. T.; Anson, A.; Gónzalez-Domínguez, J. M.; Martinez-Rubi, Y.; Simard, B. *Carbon* **2009**, *47*, 3079−3090.
(27) Dresselhaus, M. S.; Dresselhaus, G.; Saito, R.; Jorio, A. *Phys. Rep.* **2005**, *409*, 47−99.
(28) Hsieh, C.-T.; Teng, H.; Chen, W.-Y.; Cheng, Y.-S. *Carbon* **2010**, *48*, 4219−4229.

(29) Colthup, N. B.; Day, L. H.; Wiberley, S. E. In *Introduction to Infrared and Raman Spectroscopy*, 3rd ed.; Academic Press, Inc: San Diego, CA, 1990.
(30) Venkateswaran, U. D.; Rao, A. M. *Phys. Rev. B* **1999**, *59*, 10928−10934.
(31) Wu, Q.; Zhu, W.; Zahng, C.; Liang, Z.; Wang, B. *Carbon* **2010**, *48*, 1799−1806.
(32) Kashiwagi, T.; Du, F.; Douglas, J. F.; Winey, K. I.; Harris, R. H.; Shields, J. R. *Nat. Mater.* **2005**, *4*, 928−933.
(33) Fu, X.; Zhang, C.; Liu, T.; Liang, R.; Wang, B. *Nanotechnology* **2010**, *21*, 235701−235709.
(34) Hone, J.; Whitney, M.; Piskoti, C.; Zettl, A. *Phys. Rev. B* **1999**, *59*, 2514−2517.
(35) Han, Z.; Fina, A. *Prog. Polym. Sci.* **2011**, *36*, 914−944.
(36) Gonnet, P.; Liang, Z.; Choi, E. S.; Kadambala, R. S.; Zhang, C.; Brooks, J. S.; Wang, B.; Kramer, L. *Curr. Appl. Phys.* **2006**, *6*, 119−122.
(37) Kim, P.; Shi, L.; Majumdar, A.; McEuen, P. L. *Phys. Rev. Lett.* **2001**, *87*, 215502−215506.
(38) Yu, C.; Shi, L.; Yao, Z.; Li, D.; Majumdar, A. *Nano Lett.* **2005**, *5*, 1842−1846.
(39) Yu, A.; Itkis, M.; Bekyarova, E.; Haddon, R. C. *Appl. Phys. Lett.* **2006**, *89*, 133102−133105.
(40) Mott, N. F.; Davis, E. A. In *Electronic Processes in Non-Crystalline Materials*, 2nd ed.; Clarendon Press: Oxford, U.K., 1979.
(41) Jackson, R.; Domercq, B.; Jian, R.; Kippelen, B.; Graham, S. *Adv. Funct. Mater.* **2008**, *18*, 2548−2554.
(42) Parekh, B. B.; Fanchini, G.; Eda, G.; Chhowalla, M. *Appl. Phys. Lett.* **2007**, *90*, 121913−121916.
(43) Dettlaff-Weglikowska, U.; Skákalová, V.; Graupner, R.; Jhang, S. H.; Kim, B. H.; Lee, H. J.; Ley, L.; Park, Y. W.; Berber, S.; Tománek, D.; Roth, S. *J. Am. Chem. Soc.* **2005**, *127*, 5125−5131.
(44) Aldalbahi, A.; in het Panhuis, M. *Carbon* **2012**, *50*, 1197−1208.
(45) Kymakis, E.; Amaratunga, G. A. J. *J. Appl. Phys.* **2006**, *99*, 84302−84309.
(46) Coleman, J. N.; Khan, U.; Gun'ko, Y. K. *Adv. Mater.* **2006**, *18*, 689−706.
(47) Chen, W.; Feng, H.; Ye, C. *Polym. J.* **1997**, *29*, 992−996.
(48) Grein, C.; Plummer, C. J. G.; Germain, Y.; Kausch, H. H.; Béguelin, P. *Polym. Eng. Sci.* **2003**, *43*, 223−233.
(49) Spitalsky, Z.; Aggelopoulos, C.; Tsoukleri, G.; Tsakiroglou, C.; Parthenios, J.; Georga, S.; Krontiras, C.; Tasis, D.; Papagelis, K.; Galiotis, C. *Mater. Sci. Eng., B* **2009**, *165*, 135−138.
(50) Kumar, N. A.; Jeon, I. Y.; Sohn, G. J.; Jain, R.; Kumar, S.; Baek, J. B. *ACS Nano* **2011**, *5*, 2324−2331.
(51) Krenchel, H. In *Fibre Reinforcement*; Akademisk Forlag: Copenhagen, 1964.
(52) Zhao, X.; Ye, L. *J. Polym. Sci. B: Polym. Phys.* **2010**, *48*, 905−912.
(53) Yu, M. F.; Files, B. S.; Arepalli, S.; Ruoff, R. S. *Phys. Rev. Lett.* **2000**, *84*, 5552−5555.